A neurofuzzy color image segmentation method for wood surface defect detection

Gonzalo A. Ruz
Pablo A. Estévez*
Claudio A. Perez

Abstract

A crucial step in developing automated visual inspection systems for wood boards is image segmentation, which aims to achieve a high defect detection rate with a low false positive rate (clear wood areas identified as defect areas). In this study, a neurofuzzy color image segmentation method for wood surface defect detection is proposed. The method is called fuzzy min-max neural network for image segmentation (FMMIS). The FMMIS method grows boxes from a set of pixels called seeds, to find the minimum bounded rectangle (MBR) for each defect present in the wood board image. An automatic method to select seeds from defective regions as starting points to FMMIS is also presented. The FMMIS method was applied to a set of 900 images of radiata pine boards, which included samples from the following 10 categories of defects: birdseye and freckle, bark and pitch pockets, wane, splits, blue stain, stain, pith, dead knots, live knots, and holes. The FMMIS achieved a defect detection rate of 95 percent on the test set, with only 6 percent of false positives. To measure the quality of segmentation, the area recognition rate (ARR) criterion was computed using as a reference the manually placed MBR for each defect. The ARR achieved 94.4 percent on the test set. Also a relative index was used to compare the quality of segmentation between FMMIS and the segmentation module of a previously developed system, based on histogram thresholding. The results show that FMMIS allows us to obtain significant improvements compared with previous work.

In the last decades, several automated visual inspection (AVI) systems have been developed and applied to a wide range of products, including wood (Pham and Alcock 2003). AVI is an automated form of quality control normally achieved using a camera connected to a computer. The AVI framework includes five processing stages: image acquisition, image enhancement, image segmentation, feature extraction, and classification. A review of AVI research applied to the inspection of wood boards concluded that segmentation is often the most time-consuming part of the process, and that it usually does not locate all defects properly. It is necessary to develop new segmentation algorithms that can separate all defects from clear wood in the image (Pham and Alcock 1998).

Although most AVI systems for wood have been developed for gray-scale images (Pham and Alcock 1996,1998), some researchers have used color images (Conners et al. 1985, Brunner et al. 1992, Kline et al. 1998, Funck et al. 2003, Estévez et al. 2003a). Color image segmentation algorithms can be classified into one or more of the following techniques (Cheng et al. 2001): histogram thresholding, feature space clustering, region-based approaches, edge detection, fuzzy approaches, neural networks, physics-based approaches, and hybrid techniques that combine any of the techniques just mentioned. Most color segmentation approaches are based on gray level (monochrome) segmentation approaches, which can be directly applied to each component of a color space (Cheng et al. 2001). The selection of a color space is application dependent. Brunner et al. (1992) found that, for images of Douglas-fir veneer, there is no advantage in transforming the red, green, and blue (RGB) color space into other color spaces. The authors concluded that only two color parameters,

The authors are, respectively, Research Assistant and Associate Professors, Dept. of Electrical Eng., Univ. of Chile, Casilla 412-3, Santiago, Chile. The authors would like to thank Research Assistant Rodrigo Flores for his valuable help with the experiments and software implementation. This research was supported by Conicyt-Chile under grant Fondecyt 1030924. This paper was received for publication in September 2003. Article No. 9760.
*Forest Products Society Member.

Forest Prod. J. 55(4):52-58.

one measuring brightness and another chromaticity, are required to separate defects from clear wood. Funck et al. (2003) compared the performances of nine segmentation algorithms on images of Douglas-fir veneer. An algorithm that combined clustering with region-growing techniques achieved the best overall performance.

In AVI systems for wood there is usually a trade-off between the defect detection rate (true positives) and the rate of clear wood areas detected as defects (false positives). Kline et al. (1998) found that actual clear wood areas classified as defects were the primary cause for yield reduction of their prototype color AVI system. The image scanning system was very sensitive to the natural variations in the color of clear wood of red oak, and tended to identify defects that were not truly present. Pham and Alcock (1996) developed a system for segmenting gray-scale images of birch wood. The system consisted of four modules: global adaptive thresholding, multi-level thresholding, row-by-row adaptive thresholding, and vertical profiling. The results on 75 images showed a defect detection rate of 93 percent. The system had difficulty distinguishing some sound knots and hard rot from clear wood areas. In a subsequent work, a post-processing step was performed after segmentation to remove false objects and combine areas that represent the same defect, using fuzzy logic and neural network techniques (Pham and Alcock 2003). In another study, a low-cost color AVI system for classification of defects in radiata pine boards was developed (Estévez et al. 2003a). The image segmentation was performed by histogram-based multiple thresholding. The defect detection rate achieved was 95 percent. This high rate of defect detection was achieved at the expense of increasing the rate of false-positives, i.e., dark grain lines segmented as defects. One conclusion of that study was the need to enhance the segmentation process.

Artificial neural networks have been widely applied to pattern recognition tasks. A survey on image processing with neural networks reported several types of neural networks that have been applied to perform image segmentation: multilayer perceptron, self-organizing maps, Hopfield networks, probabilistic neural networks, radial basis function networks, cellular neural networks, constraint satisfaction networks, and RAM-based neural networks (Egmont-Petersen et al. 2002). On the other hand, fuzzy set theory provides a mechanism to represent and manipulate uncertainty and ambiguity. Fuzzy operators, properties, mathematics, and inference rules (*if-then* rules) have found considerable applications in image segmentation (Cheng et al. 2001). The flexibility of fuzzy sets and the computational efficiency of neural networks have caused a great amount of interest in the combination of both techniques. Among the neuro-fuzzy approaches, Simpson (1993) introduced the fuzzy min-max (FMM) clustering neural network, where clusters are represented as hyperboxes in the *n*-dimensional pattern space. The fuzzy set hyperboxes are defined by pairs of min-max points, and a membership function is defined with respect to these points. The learning algorithm is a three-step expansion-contraction process, which has the ability to learn online and in a single pass through the data.

In this work, we propose a color image segmentation method based on FMM neural networks. The new method is called fuzzy min-max neural network for image segmentation (FMMIS). The first step of the method is the automatic selection of starting pixels from defective regions. With this aim, a histogram-based study of the color intensities from defective regions and grain line regions of radiata pine boards is performed. In the second step of the method, rectangular boxes are grown from the initial set of pixels with the objective of enclosing the defective regions. The performance of the FMMIS method on the test set of pine board images is measured using the following criteria: confusion matrix, area recognition rate (ARR), average processing time, and segmentation quality. The relative ultimate measurement accuracy (RUMA) index (Zhang 1996) is used to compare the quality of segmentation between FMMIS and the segmentation module of our previously developed AVI system (Estévez et al. 2003a). Preliminary work on FMMIS applied to the segmentation of knots has been reported elsewhere (Estévez et al. 2003b).

Methods

Wood image database

A data set of 900 color images (320 by 240 pixels) of radiata pine (*Pinus radiata* D. Don) boards was drawn from the University of Chile database (Estévez et al. 2003a). The imaging system consisted of a National Television Standards Committee (NTSC) color video camera, a frame grabber from Imaging Technology, and a 333-MHz PC Pentium-II, 128 MB RAM. Lighting was a mixture of frontal halogen lights and fluorescent lamps (see Estévez et al. 2003a for details). Spatial resolution was 1.46 pixels/mm in both cross-board and down-board directions. Each image was manually labeled according to its largest defect, into one of the following 10 defect categories: birdseye and freckle, bark and pitch pockets, wane, splits, stain, blue stain, pith, dead knots, live knots, and holes. The data set, which corresponded to 90 images per category, was partitioned into two sets: 600 images for the training set and 300 images for the test set. The training set was used to adjust the FMMIS parameters. Also, 200 images from the training set were used to make the histogram-based color intensity study with samples taken from defective regions and clear wood regions. The performances of FMMIS and the segmentation module of our previous AVI system were measured on the test set.

Color of defects and grain lines

Experiments were carried out with 200 images of radiata pine boards, 20 for each defect category. For each image, samples were taken from windows of pixels belonging to defective regions and to grain lines. This was performed by manually placing the windows inside the regions of interest, from where the color intensity levels for the three RGB color channels were recorded. The window size used depended on the size of the object being analyzed. Once the sampling of the 20 boards for each category was finished, histograms were built for the intensities of pixels from defective regions and grain line areas, for each category and for each color channel. Because variable window sizes were used, the numbers of pixels from defective and grain line areas were not necessarily equal in each category. To make the histograms, the number of samples per category was chosen as the minimum value between the number of pixels from defects and the number of pixels from grain lines. The aim of this study was to obtain a range of color intensities that allow us to select pixels from defective regions,

as starting points of the proposed segmentation method.

Neurofuzzy color image segmentation method

The first step of the proposed segmentation method is to automatically locate initial pixels, called seeds, within the defective regions. Once the seeds are determined, they become the input data for FMMIS. The seed locations in the image are determined by an adaptive thresholding method, which is based on certain features of each wood board image. This allows us to take into account the great variability of the wood's color. The features used are the mean color intensity value, μ, and the minimum color intensity value, η, of the image for each channel ($t = R, G, B$).

For each color channel of the board image, a cumulative histogram, H, is constructed as follows:

$$H_t(n) = \sum_{i=\eta_t}^{n} h_t(i) \quad \text{for each } t = R,G,B \quad [1]$$

where n is the intensity level ($0 \le n \le 255$) and h_t is the histogram of the board image for channel t. Since $h_t(i) = 0$ for all $i < \eta_t$, the sum in Equation [**1**] starts from $i = \eta_t$. From the cumulative histogram an adaptive intensity level is defined as:

$$\theta_t = \alpha H(\mu_t) \quad [2]$$

where $0 \le \alpha \le 1$ is a user-defined value. Typically $\alpha \le 0.01$, since only a few pixels belonging to defective regions are searched for as seeds, and usually the defect areas cover less than 10 percent of the image. If the color intensities were constrained to be between η_t and θ_t, only the darker defects would be detected. But usually there are several defects on the same board, some brighter than others. To take into account this fact, an extra color intensity level, ξ_t, is defined as:

$$\xi_t = \frac{\theta_t + \mu_t}{2} \quad [3]$$

For each board, the seeds are taken from the following intensity range:

$$I_t = \begin{cases} [\eta_t\ \theta_t] \wedge \xi_t & \text{if } \theta_t < \lambda_t \\ [\eta_t\ \theta_t] & \text{if } \theta_t \ge \lambda_t \end{cases} \quad [4]$$

where λ_t is a user-defined threshold for each channel. The rationale underlying this parameter is that when all the defects in a board image are not too dark, the addition of an extra color intensity level (ξ_t) is not useful, and it may contribute to the detection of grain lines.

The second step is the FMMIS method, which places hyperboxes defined in the 2D geometric space by pairs of min-max points for each spatial coordinate of the image (rectangular boxes in the case of 2D images). Each hyperbox fuzzy set has an associated membership function that describes the degree of membership (spatial proximity) of a given pixel to a hyperbox in the [0,1] interval. Seeds contained within a hyperbox have full membership value, and the more separated they are from the min-max bounds of the hyperbox, the lower their membership values. When an input pattern (new seed) is presented, the hyperbox with the highest degree of membership is found and expanded to enclose the input pattern. The hyperbox expansion is accepted only if the region contained by the expanded hyperbox is similar in color to the region enclosed by the hyperbox before the expansion.

A fuzzy color homogeneity criterion is defined to compare the color similarity of two hyperboxes. This is based on a Z-function (Cheng et al. 2002) of the Euclidean distance of the mean color intensities of the two hyperboxes, measured in the RGB space. A user-defined parameter τ is introduced to control the required degree of color homogeneity for expanding hyperboxes. If the expansion criterion is not satisfied, a new hyperbox is created. An overlap test and a hyperbox contraction process are used to eliminate any overlaps formed during the construction of the hyperboxes. After a single pass through all the seeds, there is a fine-tuning hyperbox expansion process, which allows the hyperbox to grow if necessary until the defect is completely enclosed. The last stage is a hyperbox fusion process that merges hyperboxes belonging to the same defect, to ensure that each defect present in the image is contained by only one hyperbox. A membership function is used to measure the degree of spatial proximity and color similarity between two hyperboxes. If the membership value is greater than a given threshold D, the hyperboxes are merged. For more details about the FMMIS method, refer to the research by Ruz (2003).

Experimental procedure

The parameters of the adaptive thresholding method for the location of seeds as well as the parameters of FMMIS were adjusted using the training set. The seeds were ordered in a vector by traversing the image from left to right, top to bottom. When more than 100 seeds per image were obtained, this number was cut in half by taking one every other component in the seed vector. To estimate the best value of the threshold α in Equation [**2**], a receiver operating characteristic (ROC) curve was made. On an ROC graph, the true positive rate is plotted in the *y*-axis and the false positive rate is plotted in the *x*-axis, depicting the tradeoff between both rates. Values of α generating a true positive (defect detection) rate higher than 90 percent and a false positive (clear wood areas identified as defect areas) rate lower than 10 percent were searched for.

The parameters of FMMIS were set to (see Ruz 2003 for details) $\gamma = 1$ (sensitivity parameter), $\tau = 0.99$ (degree of color homogeneity used in hyperbox expansion), $u_R = 195$ (fine-tuning hyperbox expansion parameter), and $D = 0.95$ (hyperbox merging parameter). Only the red channel was used in the hyperbox fine-tuning expansion process since it performed best at separating defects from clear wood. This finding agrees with that of Brunner et al. (1992), who concluded that knots required only a measure of brightness for image analysis (red in RGB space). To avoid noisy inputs, isolated seeds having no neighboring seeds within a window of 21×21 pixels were eliminated.

The performance of the FMMIS was measured on the test set using the following criteria: confusion matrix, ARR, RUMA index of segmentation quality, and average processing time. For each of the 10 defect categories, a confusion matrix was built as shown in **Table 1**. The true positives (TP) are defined as the number of defects contained by hyperboxes, i.e., the number of defects correctly detected. The false negatives (FN) are the number of defects that are not contained by hyperboxes, i.e., the number of non-detected defects. The false positives (FP) are the number of

Table 1. — Confusion matrix.[a]

Object\hyperbox	Contained	Not contained
Defect	TP	FN
Grain line	FP	TN

[a]TP = true positives; FN = false negatives; FP = false positives; TN = true negatives.

grain lines contained by hyperboxes, i.e., the number of grain lines detected as defects. The true negatives (TN) are the number of grain lines not contained by hyperboxes, i.e., the number of non-detected grain lines. The ARR was used to measure the segmentation quality of the FMMIS. As a reference area, the minimum bounding rectangle (MBR) was manually adjusted for each defect present in the test set. The MBR is the smallest rectangle that contains all the pixels of a defect. Because most defects are not rectangular, the MBR contains all the pixels that belong to the defect plus some clear wood pixels. The ARR criterion takes into account that not necessarily all the pixels contained by a hyperbox belong to defective regions. This criterion allows us to compare the area of the hyperbox built automatically by FMMIS with the area of the manually placed MBR. The ARR is defined as:

$$ARR = \left(1 - \frac{ukp}{tp} - \frac{unp}{tp}\right) \times 100\% \quad [5]$$

where *tp* is the total number of pixels in the MBR; *ukp* is the number of unrecognized defect pixels, i.e., the absolute difference between the defect pixels contained within the MBR and the defect pixels contained within the hyperbox determined by the FMMIS method; *unp* is the number of unrecognized non-defective pixels, i.e., the absolute difference between the clear wood pixels contained within the MBR and the clear wood pixels contained within the hyperbox determined by the FMMIS method.

The performances of FMMIS and the segmentation module of our previously developed AVI system (Estévez et al. 2003a) were compared on the test set. Confusion matrices like the one shown in **Table 1** were constructed for both methods, but using the criterion of whether a defect was detected or not. To compare the segmentation quality of both methods, the RUMA index for the percent area of the defect correctly segmented, was computed as:

$$RUMA_A = \frac{|R_A - S_A|}{R_A} \times 100\% \quad [6]$$

where R_A denotes the area obtained from a reference image and S_A denotes the area measured on the segmented image. The values of $RUMA_A$ are inversely proportional to the quality of the segmentation results: the smaller the values, the better the quality regarding the feature used. The three described measures were made considering the 10 largest objects for each image. This constraint only affects the birdseye and freckle category that usually have more than 10 objects per image.

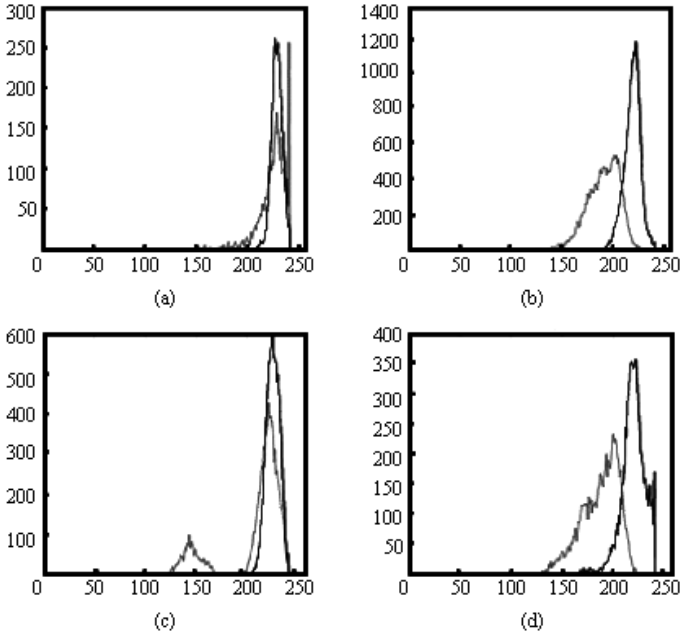

Figure 1. — Histograms from defective regions (light line) and clear wood regions (dark line) for the red channel. The samples correspond to wood boards containing the following defect categories: a) birdseye and freckle; b) blue stain; c) stain; and d) live knots.

The seeded region growing (SRG) algorithm proposed by Adams and Bischof (1994) was implemented for comparison purposes. For the wood application, an adaptive thresholding method similar to that described by Equations [**1**] and [**2**] was used to locate seeds automatically.

The neurofuzzy color image segmentation method and the SRG algorithm were implemented in MATLAB 6.5 on a PC Pentium IV, 2.4 GHz, 512 MB RAM. The average processing time was measured for each image, starting from the seed selection process and following with the respective segmentation method.

Results

As mentioned in the methods section, 200 images (20 per defect category) from the training set were used to perform a histogram-based color intensity study. **Figure 1** shows the resulting histograms for the red channel, where the dark lines represent the histograms generated from clear wood pixels and the light lines represent the histograms generated from defect pixels. The histograms overlap for most defect categories, except for the split and hole categories. The categories that showed greater overlap with clear wood were birdseye and freckle (**Fig. 1a**), blue stain (**Fig. 1b**), stain (**Fig. 1c**), and live knots (**Fig. 1d**). In general, the blue channel presented more overlapping than the other channels. For this reason, only the red and green channels were used to select starting seeds for the FMMIS method. The parameters of the adaptive thresholding method were set to $\lambda_R = 175$ and $\lambda_G = 130$ in Equation [**4**]. To set the threshold α in Equation [**2**], the ROC curve shown in **Figure 2** was plotted, using five different values of α. The best tradeoff was obtained for $\alpha = 0.007$, reaching a TP rate of 95 percent and an FP rate of 5 percent on a subset of the training set. On average, the number of selected seeds per image was about 100, i.e., 0.1 percent of the total number of pixels of an image.

Figure 3 illustrates the step-by-step application of FMMIS to an image of a radiata pine board. **Figure 3a** shows an image that contains a dead knot as a principal object and two pockets as secondary defects in the upper left part of the image. **Figure 3b** shows the seeds as white dots located within the defective regions. **Figure 3c** shows three rectangular boxes determined by the FMMIS method, after a single pass through all the seeds. **Figure 3d** shows the three boxes

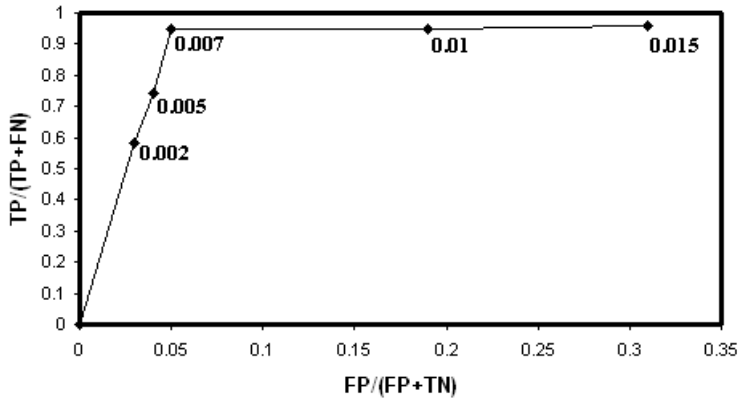

Figure 2. — ROC curve plotting TP rate versus FP rate for five different values of the parameter α, as shown on the curve. The best tradeoff is obtained for α = 0.007.

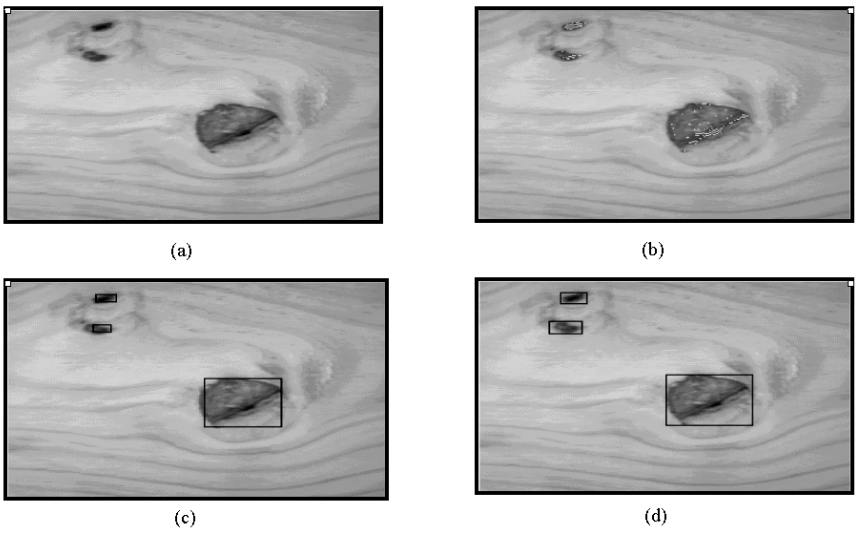

Figure 3. — Example showing the step-by-step application of the proposed color image segmentation method: a) original image containing a dead knot at the center and two pockets at the upper left; b) seeds are shown as white dots located within the defective region; c) three boxes created by FMMIS after a single pass through all seeds; and d) the same three boxes after the fine-tuning expansion process.

after the fine-tuning expansion process. **Figure 4** shows the rectangular boxes created by FMMIS on image samples of each of the 10 defect categories considered.

The FMMIS global and per category performances on the test set are summarized in **Table 2**. The TP rate achieved 95 percent of the total defects present in the test set with 10 defect categories, while the FP rate corresponded to 6 percent of the total grain lines present in the test set. The global area recognition rate achieved was 94.4 percent. The best results were obtained for the pocket, pith, dead knot, live knot, and hole categories, which presented a TP rate higher than 95 percent, an FP rate lower than 5 percent, and an ARR higher than 95 percent. The wane category achieved a perfect TP rate and ARR rate but an FP rate of 10.2 percent. Likewise, the split category achieved a TP rate of 100 percent, an ARR of 90.6 percent, and an FP level of 11.8 percent. The worst performances were obtained for the birdseye and freckle, stain, and blue stain categories, where the TP rate was lower than 95 percent, the FP rate was higher than 5 percent, and the ARR was lower than 95 percent. In contrast, the global performance of the segmentation module of our previous AVI system, which uses histogram-based multiple thresholding, obtained a TP rate of 94 percent with an FP rate of 32 percent on the same test set. None of the categories achieved an FP rate lower than 10 percent.

The $RUMA_A$ criterion was computed to compare the segmentation quality of the FMMIS and the segmentation module of our previous AVI system. **Figure 5** shows the mean value of the $RUMA_A$ index, using 30 images per category. For all defect categories, the mean values of the $RUMA_A$ index for FMMIS were smaller (better) than those for the segmentation module of our previous AVI system. A paired t-test showed that there are significant statistical differences for all categories (p-value lower than 0.05), except for the birdseye and freckle and split categories (p-value higher than 0.05).

The last column of **Table 2** shows the average processing time for FMMIS, including the seed selection process, which reached 0.11±0.04 seconds per image. In comparison, the SRG algorithm of Adams and Bischof (1994) obtained an average processing time per image of 3.03±1.30 seconds, on the same test set, i.e., FMMIS was 27 times faster than SRG. Moreover, the SRG algorithm achieved a poor segmentation on the birdseye, stain, blue stain, and split categories (TP < 50%). Only the pocket, wane, and pith categories achieved a TP rate higher than 90 percent and an FP rate lower than 6 percent.

Discussion

The segmentation module of the AVI system previously developed obtained a TP rate of 94 percent and an FP rate of 32 percent. The last figure should be compared with the FP rate of 6 percent achieved by FMMIS. This FP rate may be further reduced by filtering out boxes containing only clear wood regions. The $RUMA_A$ criterion showed that FMMIS segmented a larger proportion of the actual area of the defect than the segmentation module of our previous AVI system, for all categories except for the birdseye and freckle and split categories, which are statistically indistinguishable concerning the area of the segmented objects. The better segmentation quality of FMMIS is due to its ability to segment the complete area of the object instead of performing partial segmentation.

Table 2 shows that the worst FP rate performance corresponded to the split category. This is due to the constraint to grow boxes along the main reference system, while many splits are diagonal. For diagonal splits, the boxes would cover a large non-defective region, as can be seen in **Figure 4g**. A possible

Table 2. — Performance of FMMIS on the test set.

Defect category	TP	FN	FP	TN	TP	FP	ARR	Time
					- - - - - - - - (%) - - - - - - -			(sec.)
Birdseye and freckle	219	20	12	99	91.6	10.8	90.3	0.12
Bark and pitch pockets	34	0	3	112	100.0	2.6	95.3	0.07
Wane	34	0	11	97	100.0	10.2	100.0	0.15
Splits	40	0	18	134	100.0	11.8	90.6	0.11
Stain	40	5	9	103	88.9	8.0	84.9	0.21
Blue stain	46	5	5	65	90.2	7.1	88.2	0.13
Pith	30	0	6	137	100.0	4.2	99.8	0.13
Dead knots	37	1	3	176	97.4	1.7	99.3	0.08
Live knots	43	0	6	140	100.0	4.1	97.1	0.08
Holes	42	0	0	158	100.0	0.0	98.3	0.06
Global (10 categories)	565	31	73	1221	95	6	94.4	0.11 ± 0.04

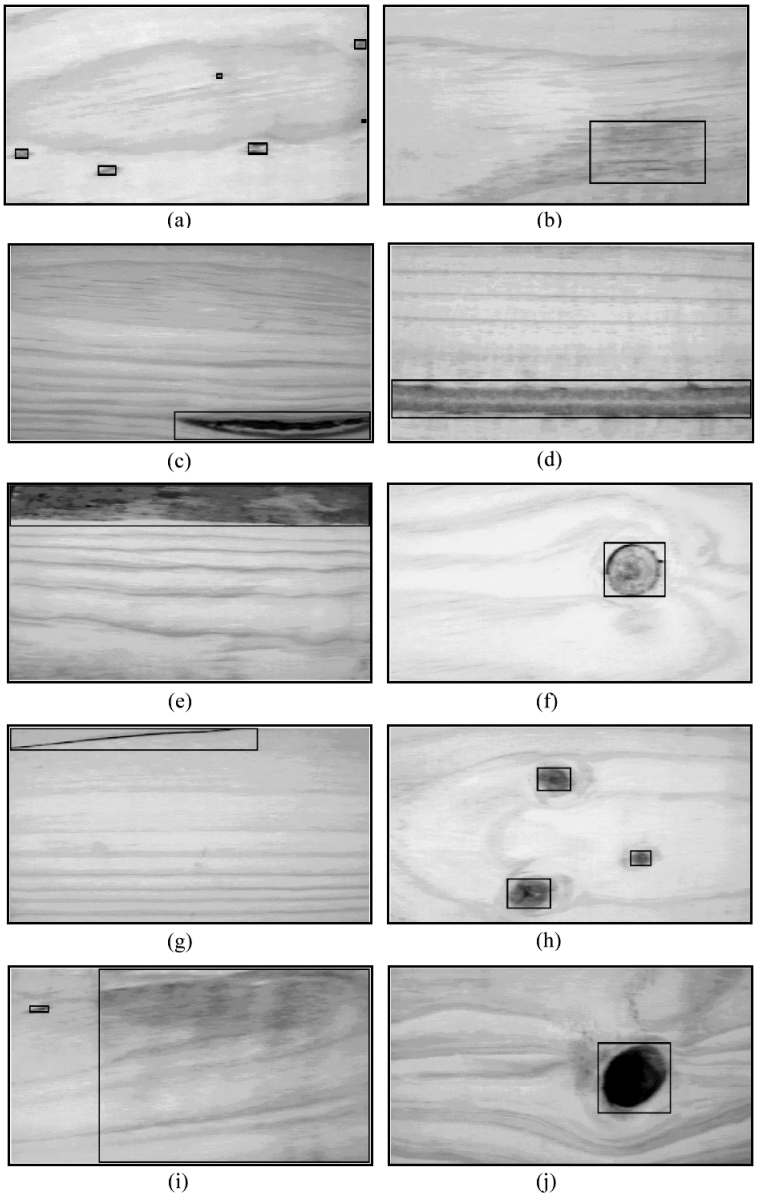

Figure 4. — Boxes determined by FMMIS on image samples for each of the 10 defect categories: a) birdseye; b) blue stain; c) pocket; d) pith; e) wane; f) dead knot; g) split; h) live knot; i) stain; and j) hole.

way of dealing with this problem is to add a box rotation stage, to allow a better fit of the box over objects that do not follow the orientation of the main reference system.

The last column of **Table 2** shows the average processing time per category. The slowest segmentation times corresponded to the stain, blue stain, wane, and pith categories. This can be explained because the FMMIS processing time depends on the number of seeds as well as the number of boxes created. Sample boards of the stain, blue stain, wane, and pith categories have typically the largest defects, and therefore tend to contain more seeds. Boards of the birdseye category have typically the greatest number of defects per image.

The processing time of the seed selection method was about one-fifth of the total processing time. Within FMMIS, the slowest stage corresponded to the merging process, which depends on the number of hyperboxes formed. The average processing time could be reduced in an order of magnitude by using C programming instead of Matlab.

Like region-growing image segmentation techniques, the FMMIS method uses a few pixels as seeds to grow regions. Nevertheless, FMMIS uses only the seeds to grow rectangular boxes, and therefore can easily expand a box to include a new seed when a color homogeneity criterion is satisfied. In contrast, the region-growing methods grow by appending to each seed all neighboring pixels that have similar properties to the seed. As a consequence, FMMIS should be faster than most region-growing methods, in particular we found that FMMIS is over 25 times faster than the SRG algorithm in the segmentation of wood defects.

The FMMIS method allows us to find the MBR of each defect present in the wood board images. This can be viewed as a coarse segmentation, aimed at quickly locating all the defect areas, and separating them from clear wood areas. Since the FMMIS algorithm is very fast (more than 25 times faster than an alternative region-growing method), there is room for a post-processing step if necessary. A fine-tuning segmentation stage could be added to find all the pixels within the MBRs that actually belong to defect areas. However, for many applications, the coarse segmentation stage may be enough, since features extracted

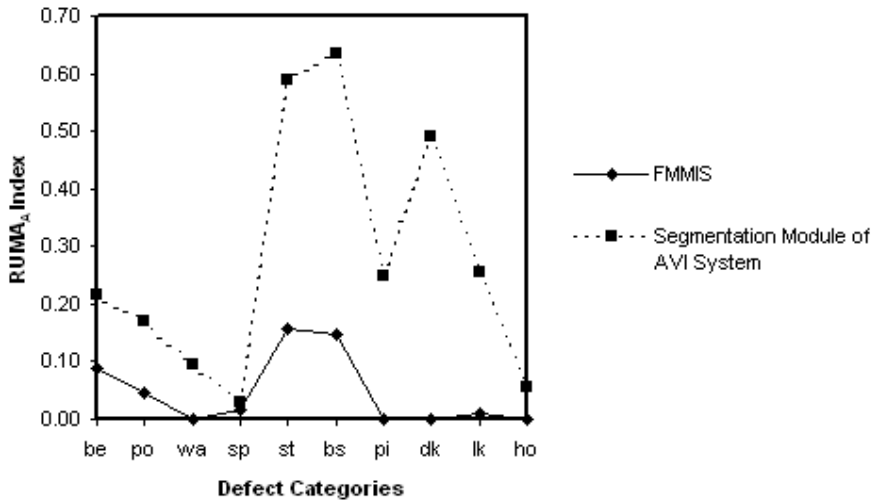

Figure 5. — Comparison of the quality of segmentation between FMMIS and the segmentation module of the AVI system previously developed (Estévez et al. 2003a), under the average RUMA index for the area of the segmented objects. Letters on the x-axis correspond to one of the 10 defect categories: birdseye (be), pocket (po), wane (wa), split (sp), stain (st), blue stain (bs), pith (pi), dead knot (dk), live knot (lk), and hole (ho).

from the MBRs could be directly used to classify the segmented objects into one of the 10 defect categories. Once the defects have been located and identified, the cutting process at the rough mill has to follow the main reference system, as the edges of the MBRs do.

Conclusions

The proposed color image segmentation method achieved a high defect detection rate (95%) with a low false positive rate (6%) on images of radiata pine boards. A key part of the method is the automatic selection of seeds belonging to defective regions, which is based on adaptive thresholding. The seed selection procedure may be easily adjusted to other kinds of wood, with different illumination systems, by analyzing the histograms of wood samples.

The results show that significant improvements have been obtained, in comparison with previous work, regarding the isolation of defects from clear wood and the quality of the segmentation of defects on images of radiata pine boards.

Literature cited

Adams R. and L. Bischof. 1994. Seeded region growing. IEEE Trans. Pattern Anal. Machine Intell. 16(6):641-646.

Brunner, C.C., A.G. Maristany, D.A. Butler, D. VanLeeuwen, and J.W. Funck. 1992. An evaluation of color spaces for detecting defects in Douglas-fir veneer. Industrial Metrology 2: 169-184.

Cheng, H.D., X.H. Jiang, and J. Wang. 2002. Color image segmentation based on homogram thresholding and region merging. Pattern Recognition 35:373-393.

_____, _____, Y. Sun, and J. Wang. 2001. Color image segmentation: Advances and prospects. Pattern Recognition 34:2259-2281.

Conners R.W., C.W. McMillin, and C.N. Ng. 1985. The utility of color information in location and identification of defects in surfaced hardwood lumber. *In*: Proc. of the First Inter. Conf. on Scanning Technology in Sawmilling. Miller-Freeman Publications, Forest Prod. Soc., Madison, WI. pp. XVIII 1-33.

Egmont-Petersen, M., D. de Ridder, and H. Handels. 2002. Image processing with neural networks - A review. Pattern Recognition 35: 2279-2301.

Estévez, P.A., C.A. Perez, and E. Goles. 2003a. Genetic input selection to a neural classifier for defect classification of radiata pine boards. Forest Prod. J. 53(7/8):87-94.

_____, G.A. Ruz, and C.A. Perez. 2003b. Fuzzy min-max neural network for image segmentation. *In*: Proc. of the 7th Joint Conf. on Information Sci. (JCIS 2003). Assoc. for Intelligence Machinery, Durham, NC. pp. 655-659.

Funck, J.W., Y. Zhong, D.A. Butler, C.C. Brunner, and J. P. Forrer. 2003. Image segmentation algorithms applied to wood defect detection. Comput. Electron. Agr. 41(1-3): 157-179.

Kline, D.E., A. Widoyoko, J.K. Wiedenbeck, and P.A. Araman. 1998. Performance of color camera machine vision in automated furniture rough mill systems. Forest Prod. J. 48(3): 38-45.

Pham, D.T. and R.J. Alcock. 1996. Automatic detection of defects on birch wood boards. *In*: Proc. Institution of Mechanical Engineers, Part E. J. of Process Mechanical Engineering 210:45-52.

_____ and _____. 1998. Automated grading and defect detection: A review. Forest Prod. J. 48(4):34-42.

_____ and _____. 2003. Smart Inspection Systems. Academic Press, London. 218 pp.

Ruz, G.A. 2003. New color image segmentation method based on fuzzy min-max neural networks. MS thesis. Dept. of Electrical Engineering, Univ. of Chile, Santiago, Chile. 88 pp. (in Spanish).

Simpson, P.K. 1993. Fuzzy min-max neural networks. Part 2. Clustering. IEEE Trans. Fuzzy Sets 1:32-45.

Zhang, Y.J. 1996. A survey on evaluation methods for image segmentation. Pattern Recognition 29(8):1335-1346.